© Pol J Radiol 2026; 91: e195-e204
DOI: https://doi.org/10.5114/pjr/216134

Received: 07.10.2025
Accepted: 27.12.2025
Published: 22.04.2026

Polish Journal of Radiology
http://www.polradiol.com

Original paper

Differentiation of cervical cancer subtypes using machine learning models on MRI images

Asiye Sozeri[1,A,B,C,D,E,F,G], Neslihan Gokmen[2,C,D], Eda Kayali[3,B,D], Zeliha Firat Cuylan[3,A,E,F,G], Fatih Eroglu[1,A,E,F], Izzet Selcuk Parlak[4,A,B], Gunsu Kimyon Comert[3,A,D,E,F,G]

[1]Department of Radiology, Karabük Training and Research Hospital, Karabuk, Turkey
[2]Computer Engineering Department, College of Engineering, Koc University, Istanbul, Turkey
[3]Department of Gynecologic Oncology, Ankara Bilkent City Hospital, Ankara, Turkey
[4]Department of Radiology, Ankara Bilkent City Hospital, Ankara, Turkey

Abstract

Purpose: To develop and compare various radiomics-based machine learning (ML) models for distinguishing cervical squamous cell carcinoma (SCC) from non-SCC histopathological subtypes, using multiparametric magnetic resonance imaging (MRI) and clinical data.

Material and methods: This retrospective study included 88 women (mean age, 51.1 ±13.0 years; range, 25-83 years) with histopathologically confirmed cervical cancer (47 SCC, 41 non-SCC). For each patient, axial and sagittal T2-weighted imaging (T2WI) and diffusion-weighted imaging (DWI) were available, along with clinical metadata. Radiomic features (shape, first-order, and texture features including gray-level co-occurrence matrix, gray-level run length matrix, and gray-level size zone matrix) were extracted from each sequence, yielding 945 features per patient. A feature set was created by combining features from all three sequences. The least absolute shrinkage and selection operator (LASSO) method was used for feature selection. Three supervised classifiers – random forest (RF), support vector machine (SVM), and logistic regression (LR) – were trained to classify SCC versus non-SCC.

Results: Among the single-sequence models, the sagittal T2WI sequence demonstrated the strongest performance, achieving receiver operating characteristic (ROC) area under the curve (AUC) values of 0.839 with SVM and 0.732 with LR. In contrast, the axial T2WI RF model showed poor discriminative ability (ROC-AUC: 0.464), indicating that this sequence alone provides limited value for subtype differentiation despite showing acceptable accuracy metrics. The combined multi-sequence model yielded the highest overall performance. Using LASSO-selected features, RF achieved the best ROC-AUC (0.958), followed closely by SVM (0.953) and LR (0.951), with all models attaining accuracies above 0.91.

Conclusions: Feature-level integration of axial T2WI, sagittal T2WI, and DWI substantially enhances ML performance in differentiating SCC from non-SCC cervical cancer subtypes. Compared with single-sequence models, the combined multi-sequence approach provides more robust and well-balanced classification, underscoring the complementary value of multiparametric MRI for histopathological subtype prediction.

Key words: cervical cancer, MRI, radiomics, squamous cell carcinoma, machine learning.

Introduction

Cervical cancer is the fourth most common malignancy among women worldwide [1]. The two primary histological subtypes are squamous cell carcinoma (SCC) and adenocarcinoma (AC), accounting for approximately 70-75% and 10-25% of cases, respectively. Notably, the incidence of AC has been steadily rising over recent decades [2]. Understanding the distinctions between AC and SCC from multiple perspectives is essential, as these differences can

Correspondence address:
Asiye Sozeri, Department of Radiology, Karabuk Training and Research Hospital, 1 Alpaslan St., 78200 Karabuk, Turkey, e-mail: asisozeri@gmail.com

Authors' contribution:
A Study design · **B** Data collection · **C** Statistical analysis · **D** Data interpretation · **E** Manuscript preparation · **F** Literature search · **G** Funds collection

inform more personalized treatment strategies. Wu *et al.* demonstrated that treatment modality influences survival outcomes in cervical cancer depending on histopathological subtype, with surgery offering a survival advantage in AC [3].

Pathological examination remains the gold standard for diagnosing cervical cancer [4]. Considering the limited availability of pathologists, delays in pathology reporting, substantial workload demands, observer variability, and the additional time and cost associated with immunohistochemical analyses, there is a growing need for tools capable of providing faster and more standardized diagnostic outcomes. Distinguishing between AC and SCC using the current standard imaging methods – such as magnetic resonance imaging (MRI), positron emission tomography/computed tomography (PET/CT), and ultrasound (USG) – remains a challenge for radiologists, often resulting in low interobserver consistency [5,6].

MRI is the preferred imaging modality for the pretreatment staging of cervical cancer and plays a central role in contemporary management algorithms. Its superior soft-tissue contrast enables accurate evaluation of tumor size, depth of stromal invasion, parametrial and vaginal extension, as well as adjacent organ involvement – features that constitute key components of the International Federation of Gynecology and Obstetrics staging system and serve as critical determinants in treatment planning [7].

Radiomics, an emerging and rapidly evolving field of research, addresses this challenge by extracting quantitative information from medical images and transforming it into high-dimensional datasets for advanced analysis. This approach allows a more comprehensive characterization of disease features and provides substantial support for clinical decision-making [8,9]. Medical imaging is widely used to facilitate the diagnosis and staging of numerous conditions; in cervical cancer, pretreatment MRI is typically performed to evaluate the tumor, monitor its progression, and assess treatment response [10,11]. However, radiological interpretation remains inherently subjective and cannot provide the definitive, objective accuracy offered by histopathological evaluation. There remains a notable lack of studies evaluating postoperative outcomes in patients with SCC compared with those with non-SCC subtypes.

In this research, we aimed to examine the potential use of multiparametric MRI-based radiomics analysis in distinguishing cervical cancer histopathological subtypes, particularly SCC versus non-SCC.

Material and methods

Study subjects and subject screening

Between May 2019 and September 2024, 113 patients who underwent MRI for suspected cervical mass or histopathologically confirmed cervical cancer were identified. Among those, 25 were excluded, either due to loss to follow-up after imaging ($n = 10$), or non-diagnostic image artifacts on cervical protocol MRI ($n = 5$), or millimetric tumors not detectable on MRI ($n = 10$) (Figure 1). MRI examinations, including T1-weighted imaging (T1WI), T2-weighted imaging (T2WI), diffusion-weighted imaging (DWI) and dynamic contrast-enhanced (DCE)-MRI, were performed prior to surgery. Ultimately, 88 patients with cervical cancer (47 SCC and 41 non-SCC) were included in the study. This retrospective study was approved by the institutional ethics committee (approval No. 2/25/889).

MRI acquisition and processing

All patients underwent SIGNA 3T MRI scans prior to surgical treatment. Patients were advised to fast for 8-10 hours prior to examination and were positioned supine with a partially full bladder. The scanning range was appropriately aligned with the cervix, extending from the upper edge of the iliac crest to the level of the bilateral femoral neck, with the axial scanning plane perpendicular to the long axis of the cervix. The imaging sequences included T1WI, T2WI, DWI ($b = 50$, 800, 1400), and DCE-MRI. Sagittal T2WI was acquired with a repetition time (TR)/echo time (TE) of 2980/106 ms, field of view of 256 × 320 mm and a slice thickness of 3.5 mm. Axial T2WI, oriented perpendicular to the long axis of the cervical canal, was obtained with a TR/TE of 4600/114 ms, field of view of 384 × 288 mm and a slice thickness of 3.3 mm. DWI was performed in the axial plane using single-shot echo-planar imaging with b-values of 50, 800, 1400 s/mm^2, TR/TE of 2000/79 ms, field of view of 110 × 44 mm, and a slice thickness of 5 mm.

The MRI images (sagittal T2WI, axial T2WI, DWI) of the patients included in the study were uploaded from the hospital's picture archiving and communication system to the 3DSlicer Version 5.2.2 program stored in the hospital's internal network. The region of interest was obtained from the area where the largest dimension

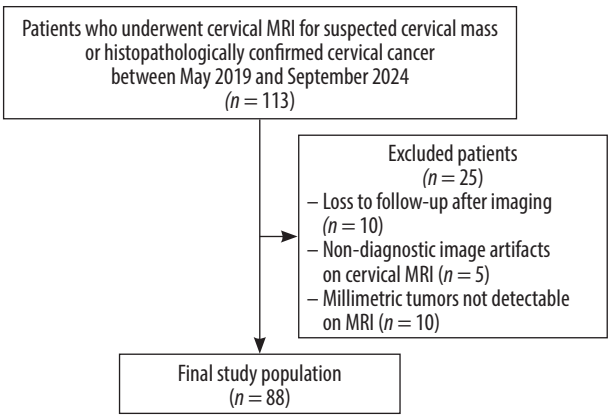

Figure 1. Flowchart of patient selection

MRI – magnetic resonance imaging

of the lesion was located on each sequence. Tumor segmentation was performed by a radiologist with 5 years of experience in gynecological imaging and reviewed by a senior radiologist with over 15 years of experience in gynecological imaging. MRI images and segmentations of patients diagnosed with different types of cervical cancer are shown in Supplement Images 1, 2 and 3.

Statistical analysis

Dataset

To evaluate the combined impact of multimodal data fusion, a combined dataset was created which included features from all three sequences. Using a typical radiomics pipeline comprising shape, first-order statistics, and texture features – such as gray-level co-occurrence matrix (GLCM), gray-level run length matrix, and gray-level size zone matrix – the dataset contained 945 extracted radiomic features per patient. Age was a structured variable in the clinical information. For modeling purposes, the target variable was converted into a binary classification problem. The mean imputation technique was used to impute all missing variables. To guarantee uniform scaling across characteristics, radiomic and clinical features were then independently normalized using *z*-score normalization (standard scaler).

Model training and feature selection

Using radiomic and clinical characteristics, three supervised machine learning (ML) classifiers were used to distinguish between distinct subtypes of cervical cancer: random forest (RF), support vector machine (SVM), and logistic regression (LR). These classifiers were trained using the combined dataset and each MRI sequence (axial T2WI, sagittal T2WI, and DWI). The least absolute shrinkage and selection operator (LASSO) approach was used for feature selection, as it is particularly well suited for high-dimensional radiomic data and helps minimize overfitting while improving model interpretability. By reducing the weights of less informative features to zero, LASSO promotes sparsity by applying an L_1 penalty to the regression coefficients. The definition of the optimization problem is:

$$\min_{\beta} \left\{ \frac{1}{2n} \sum_{i=1}^{n} (y_i - X_i\beta)^2 + \lambda \sum_{j=1}^{p} |\beta_j| \right\}$$

where y_i is the binary target label, X_i is the feature vector, β_j are the model coefficients and λ is the regularization parameter [12]. Hyperparameter optimization for all models was performed using GridSearchCV with 5-fold stratified cross-validation, optimizing for receiver operating characteristic (ROC) area under the curve (AUC). The dataset was split into 80% training and 20% test sets, maintaining the label distribution using stratified sampling. All implementations were carried out in Python (v3.9) using the Scikit-learn library.

Evaluation metrics

Both probabilistic (ROC-AUC) and threshold-based metrics (accuracy, precision, recall, and F1-score) were used to evaluate classification performance. All metrics are based on the confusion matrix components:

$$\text{Accuracy} = \frac{TP + TN}{TP + FP + TN + FN}$$

$$\text{Precision} = \frac{TP}{TP + FP}$$

$$\text{Recall} = \frac{TP}{TP + FN}$$

$$\text{F1-score} = \frac{2 \times (\text{Precision} \times \text{Recall})}{(\text{Precision} + \text{Recall}}$$

False negative (FN), true negative (TN), false positive (FP) and true positive (TP) samples were used for calculation. The F1-score, which is particularly useful for imbalanced datasets and is calculated as the harmonic mean of precision and recall, was used. For imbalanced classes, the area under the precision–recall curve (AUC-PRC), which evaluates the trade-off between precision and recall across thresholds and provides greater utility than ROC-AUC, was used [13]. From the ML classifiers, feature importance was derived for the radiomic features that contributed most. To identify multicollinearity and possible redundancy, radiomic characteristics were correlated using Pearson correlation analysis. Because of the nature of the data (no repeated measures design), Pearson correlation analysis was used instead of intra-class correlation coefficient analysis to evaluate dependability among radiomic characteristics.

Results

The best-performing parameters for the axial T2WI sequence were found as follows: RF with 100 trees, maximum depth of 5, and minimum samples per split set to 5; LR with a regularization strength C = 100; and SVM with a linear kernel and C = 1. For the sagittal T2WI sequence, optimal parameters included: RF with the same configuration as above; LR with C = 100; and SVM with radial basis function (RBF) kernel and C = 0.1. On the DWI sequence, the best settings were: RF with 100 estimators, maximum depth of 5, and minimum samples per split set to 2; LR with C = 100; and SVM with an RBF kernel and C = 10. For the combined model incorporating features from all sequences, the RF achieved the best results with 200 estimators, maximum depth of 5, and minimum samples

per split of 2; LR performed best with a more regularized setting C = 0.01; and the optimal SVM configuration used an RBF kernel with C = 1. To impose sparsity and reduce overfitting, LASSO regularization was used for the initial high-dimensional radiomic features. The RF, SVM, and LR models were then trained on all MRI sequences using the 88 predictive features with non-zero coefficients that were produced by this process.

The classification performance for several MRI sequences and classifiers is summarized in Table 1. In the axial T2WI sequence, RF models had low precision (0.60) compared to LR and SVM (0.86), and also showed poor ROC-AUC (0.464), despite achieving higher accuracy and F1-scores in other MRI sequences.

In the sagittal T2WI sequence, SVM achieved the highest accuracy (83%), F1-score (82%), and ROC-AUC (0.839). It was also associated with strong balance between recall and precision. LR and RF both achieved moderate performance, with accuracy around 78% and lower F1-scores. However, these values were inferior to SVM. The ROC-AUC values for all classifiers in sagittal T2WI (0.732-0.839) were markedly higher than those obtained from axial T2WI (0.375-0.464).

RF achieved the highest performance among the classifiers for DWI, with an accuracy of 83%, F1-score of 82%, and ROC-AUC of 0.634. Comparing across sequences, DWI was inferior to sagittal T2WI in terms of ROC-AUC (0.634-0.679 vs. 0.732-0.839), but still superior to axial T2WI (0.375-0.464).

Among all the classifiers, the combined sequence model that incorporated features from axial, sagittal, and DWI images demonstrated the best classification performance. RF achieved the highest accuracy (92%), with excellent precision (93%), recall (92%), F1-score (92%), and a near-perfect ROC-AUC of 0.958 for combined sequence. SVM also performed extremely well, with an accuracy of 91%, precision of 92%, recall of 91%, F1-score of 90%, and ROC-AUC of 0.953 in combined sequence. LR yielded comparable performance, with accuracy of 91%, precision of 91%, recall of 91%, F1-score of 91%, and ROC-AUC of 0.951. In contrast to the variable and sometimes limited results of the individual sequences, the combined approach produced uniformly high values across all metrics, with minimal differences between classifiers.

Strong classification performance with reasonably balanced sensitivity and specificity is demonstrated by the confusion matrices of the ML classifiers trained on combined radiomics features, as shown in Figure 2. With high TP and TN rates, the RF model achieved the optimum agreement, correctly detecting 28 out of 28 SCC instances and 21 out of 25 non-SCC cases. With a slightly higher number of FN (5), the LR model likewise demonstrated strong performance, accurately identifying all SCC instances (28/28) and 20 of the 25 non-SCC cases. With just one FN and four FP, the SVM model also showed good discrimination; in terms of sensitivity, it approximately matched RF.

All three ML classifiers trained on LASSO-selected radiomics features from the concatenated sequences show high discriminative ability, as indicated by the ROC curves in Figure 3. Accordingly, the RF, LR, and SVM classifiers achieved ROC-AUC values of 0.96, 0.95, and 0.95, respectively, in distinguishing between SCC and non-SCC groups.

In the RF model trained on the combined MRI sequences, the most informative radiomic features included Strength, GrayLevelNonUniformityNormalized, Busyness, ClusterTendency, LargeAreaLowGrayLevelEmphasis, and JointEnergy, as illustrated in Figure 4.

The Pearson correlation heatmap for the top 20 radiomic characteristics with the highest inter-feature correlations is shown in Figure 5. The matrix shows that a large

Table 1. Overall test performances of the machine learning architectures for different magnetic resonance imaging (MRI) sequences

MRI Sequence	Classifier	Accuracy	Precision	Recall	F1-score	ROC-AUC
Axial T2WI	RF	0.78	0.6	0.78	0.68	0.464
	LR	0.83	0.86	0.83	0.79	0.393
	SVM	0.83	0.86	0.83	0.79	0.375
Sagittal T2WI	RF	0.78	0.60	0.78	0.68	0.750
	SVM	0.83	0.82	0.83	0.82	0.839
	LR	0.78	0.78	0.78	0.78	0.732
DWI	RF	0.83	0.82	0.83	0.82	0.634
	SVM	0.67	0.78	0.67	0.69	0.679
	LR	0.78	0.74	0.78	0.75	0.500
Combined	RF	0.92	0.93	0.92	0.92	0.958
	SVM	0.91	0.92	0.91	0.90	0.953
	LR	0.91	0.91	0.91	0.91	0.951

AUC – area under the curve, LR – logistic regression, RF – random forest, ROC – receiver operating characteristic, SVM – support vector machine, T2WI – T2-weighted imaging

number of features have substantial correlations, with correlation coefficients higher than 0.95.

Discussion

The main findings of this study indicate that the sagittal T2WI sequence provides greater diagnostic value than the axial sequence. In particular, the SVM classifier not only achieved accurate classification in most cases but also demonstrated a strong balance between sensitivity and precision on sagittal T2WI, making it especially effective for distinguishing SCC from non-SCC cases across a range of probability thresholds. Moreover, the integration of multiple MRI sequences consistently yielded superior performance, regardless of the classifier used. When features from axial T2WI, sagittal T2WI, DWI, and potentially DCE-MRI were combined, all ML classifiers showed markedly improved performance compared with models trained on any single sequence alone. In the combined model, RF had a slightly higher AUC compared to LR and SVM, but the difference was minimal.

The most accurate image of the typical regional anatomy of the cervix is found on T2WI, where the mucosa and central endocervical glands exhibit hyperintense signal intensity, surrounded by hypointense fibrous stroma and loose stroma that extends to the parametrium with intermediate signal intensity [14]. Cervical tumors, when identifiable on imaging, are most clearly visualized on T2WI, typically presenting as lesions with intermediate signal intensity that stand out against the low-signal cervical stroma. DWI can further facilitate tumor detection, particularly in cases where the lesion appears isointense relative to the surrounding cervical tissue. Several studies have highlighted the incremental benefit of DWI for identifying tumors at initial staging – especially small lesions that may be subtle or isointense on T2WI – as well as for improving the detection of recurrent cervical cancer [15]. In line with the most recent European Society of Urogenital Radiology guidelines, T2WI and DWI constitute the core sequences for cervical cancer MRI. These sequences should ideally be acquired with matching planes, field of view, and slice thickness to enable optimal side-by-side assessment. They are considered essential for initial staging, evaluation of treatment response, and surveillance for recurrence. By contrast, the same recommendations indicate that DCE-MRI may be used selectively and remains optional [16]. Consistent with current recommendations, our study incorporated axial and sagittal T2WI together with DWI.

Tumor heterogeneity is an important prognostic factor, as greater heterogeneity is often associated with enhanced aggressiveness, resistance to therapy, and poorer clinical outcomes [17]. Cervical cancer, in particular, shows considerable heterogeneity at both genetic and histopathological levels [8,18]. Among prognostic factors, histopathological subtype plays a crucial role, as different subtypes

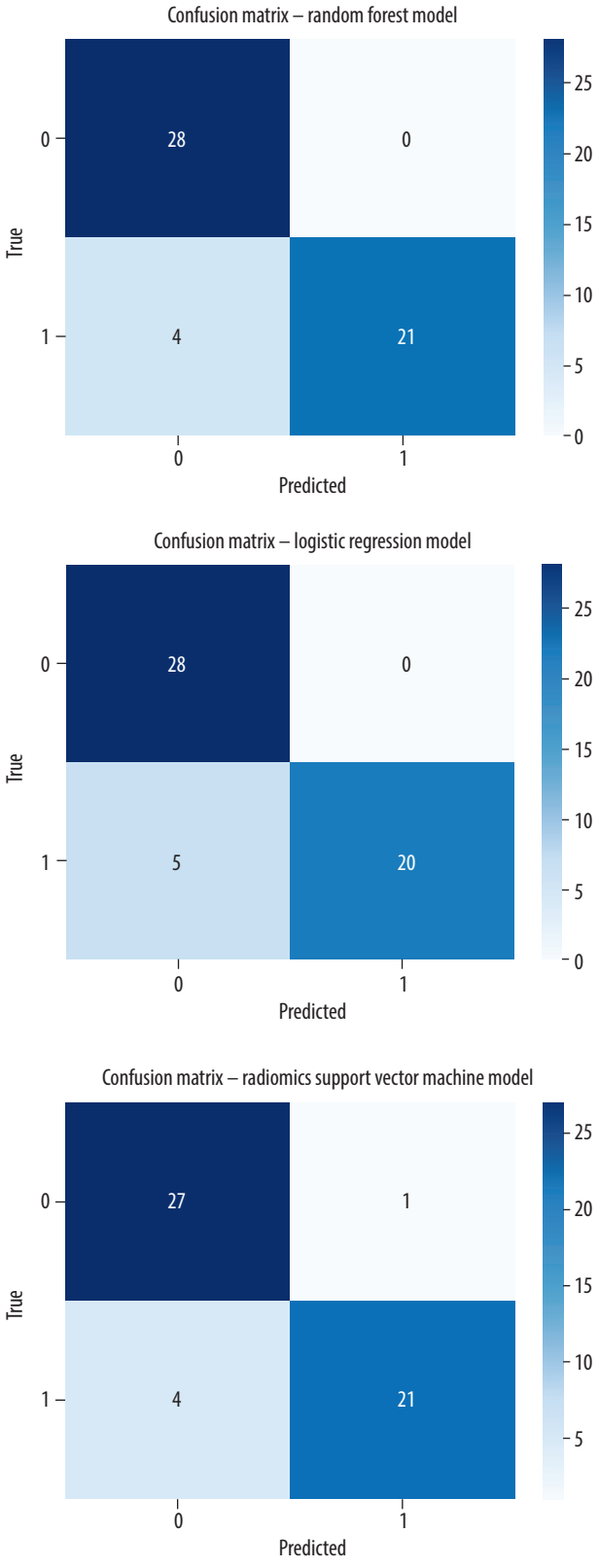

Figure 2. Confusion matrix for machine learning (ML) architectures of combined sequences

are characterized by distinct biological behaviors [19]. Although current National Comprehensive Cancer Network guidelines do not provide different treatment strategies for SCC and AC [20], multiple studies have indicated that AC is associated with a less favorable prognosis [21-23].

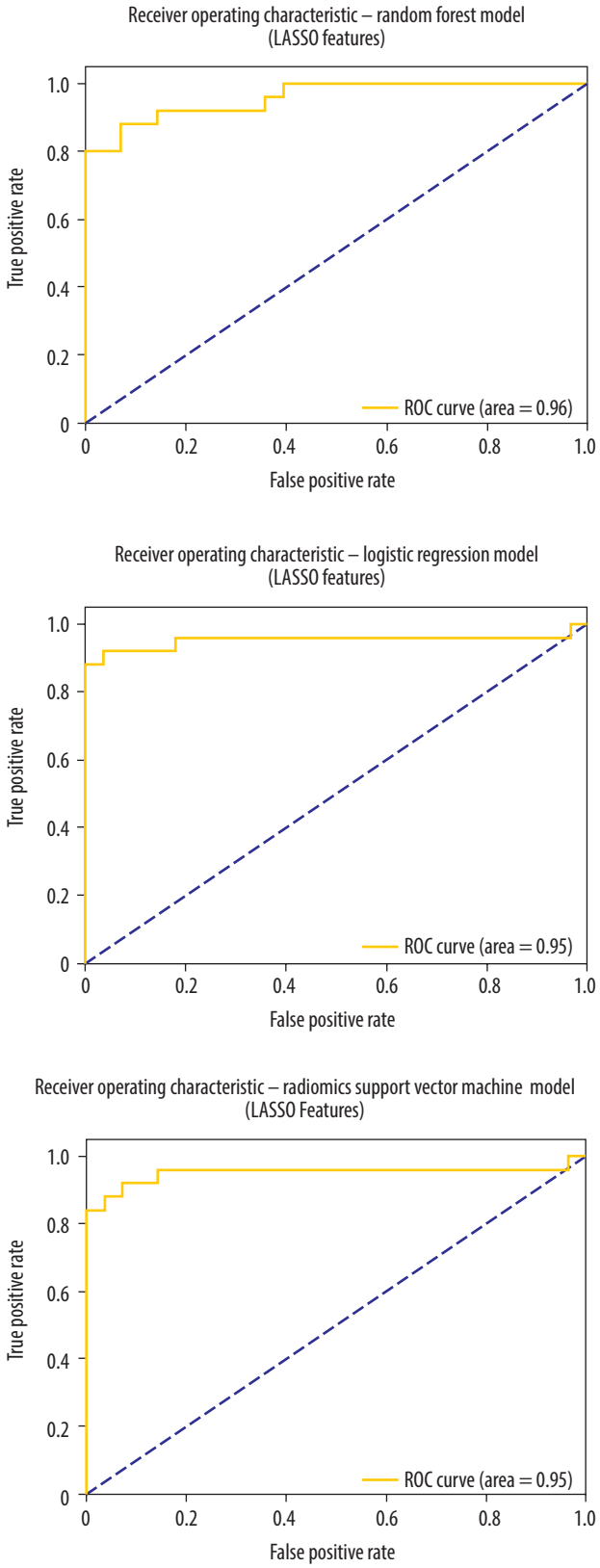

Figure 3. Receiver operating characteristic (ROC) for machine learning (ML) architectures of combined sequences

Compared to SCC at the same stage, AC tends to be more aggressive, less responsive to chemoradiotherapy, and more prone to metastasis, resulting in poorer outcomes and lower survival rates [21-23]. Therefore, acknowledging these differences is essential for developing precise and individualized treatment strategies, highlighting the importance of subtype-oriented clinical approaches.

Although pathological examination remains the gold standard for subtype differentiation, it has several limitations, including inherent subjectivity, interobserver variability, the need for additional consultation among pathologists, and, in certain cases, the requirement for supplementary immunohistochemical staining – all of which increase both time and cost. Moreover, as pathology relies on small tissue samples, inadequate specimens may necessitate repeated biopsies, leading to additional invasive procedures and further delays. In contrast, radiomics-based, non-invasive imaging may provide potential advantages such as reducing biopsy-related risks, capturing the entire tumor heterogeneity, rather than a limited sample, enabling earlier treatment planning, and potentially reducing time and cost in the long term. However, distinguishing cervical cancer subtypes and assessing tumor heterogeneity remain difficult tasks when relying on conventional non-invasive imaging techniques [8]. Several studies have employed MRI with DWI or fluorodeoxyglucose PET/CT [5,21,24-28]. Some studies showed that the apparent diffusion coefficient (ADC) values were significantly lower in SCC compared to AC [5,21,24], whereas others found no statistically significant differences between the two subtypes [28]. Non-SCC tumors tend to be less conspicuous on MRI, making them more difficult to detect compared to SCC. Consequently, attempts have been made to separate SCC from non-SCC tumors using various imaging modalities [29-31]. This reduced visibility may lead to false negative interpretations, potentially resulting in an underestimation of the required surgical resection. More recently, radiomics has gained attention as a promising tool, enabling the extraction of high-dimensional quantitative features from imaging platforms such as MRI, CT, PET, and USG. By capturing subtle imaging patterns beyond visual assessment, radiomics provides deeper insights into tumor biology and holds considerable potential for diagnostic, prognostic, and predictive applications [32].

In a study by Wang *et al.*, radiomic features derived from three MRI sequences, including T2WI and ADC maps, demonstrated that ACs exhibit greater tissue heterogeneity compared to SCCs; however, shape-based features did not show significant differences between the two histological subtypes [33]. A total of 105 radiomic features were extracted, many of which showed significant differences between AC and SCC. Notably, the sagittal T2WI sequence achieved the highest individual AUC of 0.86. Furthermore, a radiomics model integrating features from five MRI sequences outperformed any single sequence, achieving an AUC of 0.89, with an accuracy of 0.81, sensitivity of 0.67, and specificity of 0.94, highlighting the enhanced discriminative potential of a multi-parametric radiomics approach [33]. In a retrospective study conducted by

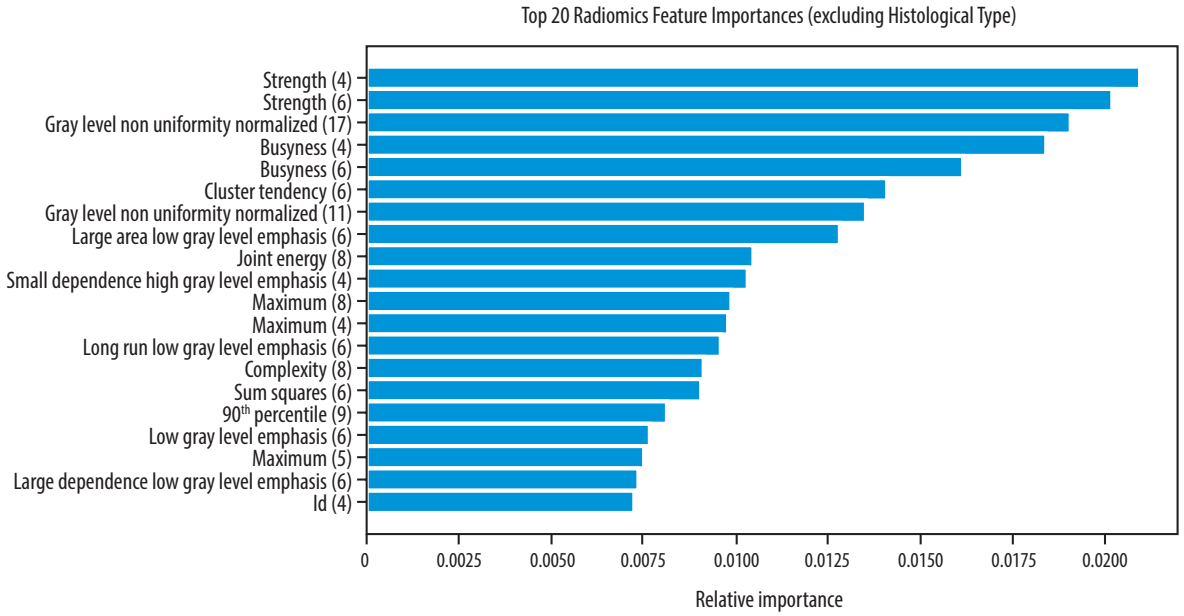

Figure 4. Top 20 Radiomics Feature Importance obtained from random forest (RF) combined sequence

Wang *et al.* [34], a multi-parameter MRI-based radiomic signature was developed and validated for the diagnosis of low-differentiated and high-differentiated cervical SCC. Radiomic signatures derived from the combination of DWI and T2WI demonstrated better clinical utility. To distinguish between low-differentiated and high-differentiated cervical SCC, the AUC reached 0.844 in the training cohort, and 0.822 in the validation cohort. In our study, the accuracy for distinguishing SCC from non-SCC subtypes was high (0.92), and the performance of the ML models, along with the evaluation metrics, further demonstrated strong overall diagnostic capability. Unlike previous studies, our analysis additionally included precision, recall, F1-score, and ROC-AUC metrics, resulting in promising outcomes. In our study, combined MRI sequences, based on the combination of all three sequences, instead of a single MRI sequence, yielded the best results through LR, SVM, and RF classifiers from ML models. Among these models, the RF model derived from combined sequences demonstrated the best performance, achieving accuracy, precision, recall, F1-score, and ROC-AUC values of 0.92, 0.93, 0.92, 0.92, and 0.958, respectively. The RF classifier achieved excellent performance, with the highest ROC-AUC of 0.958 and an accuracy of 0.91, outperforming the SVM (0.953) and LR (0.951) models, though the difference was minimal. These results represent the highest performance reported in the literature for the differentiation of cervical cancer subtypes.

GLCM-based features, particularly cluster tendency, busyness, and strength, highlight that textural heterogeneity is critical for differentiating SCC from other histopathological types. Tumor homogeneity and structural irregularity, reflected in zone emphasis and gray-level non-uniformity metrics, serve as important diagnostic indicators. These findings demonstrate that multi-sequence MRI-derived radiomic signatures can identify subtle but distinct imaging biomarkers linked to the pathophysiology of cervical tumors. GLCM features capture comprehensive information about spatial distribution, including direction, distance, gray-level intensity, and structural patterns, with higher scores indicating greater heterogeneity [35].

Unlike previous MRI studies, our analysis revealed significant redundancy among certain radiomic features, as highlighted in the Pearson correlation heatmap. Features such as Difference Entropy, Interquartile Range, Mean Absolute Deviation, and 90th Percentile frequently exhibited strong mutual correlations. To prevent multicollinearity and overfitting in ML models, dimensionality reduction or feature selection methods such as LASSO are necessary. Overall, cervical tumor radiomic profiles appear to be dominated by specific texture and intensity patterns, reflected in tightly clustered feature groups.

Limitations

This study has several limitations. First, it was conducted retrospectively; selection bias cannot be excluded. Second, due to its single-center design, the sample size was relatively limited; however, given that the study was conducted at a tertiary cancer center with a high patient volume and experienced radiology staff, the sample size was still reasonable for a single-center study. Variability in MRI acquisition and segmentation protocols may also affect feature reproducibility. Despite using LASSO for feature selection, the high-dimensional radiomic data carry an inherent risk of overfitting. Nevertheless, the study demonstrates notable strengths. By integrating multi-sequence MRI radiomics (axial T2WI, sagittal T2WI, and DWI), ML classifiers (RF, SVM, LR) achieved excellent accuracy, precision, recall, F1-score, and ROC-AUC values, with RF reaching a near-perfect ROC-AUC of 0.958. Comprehensive evaluation metrics and analysis

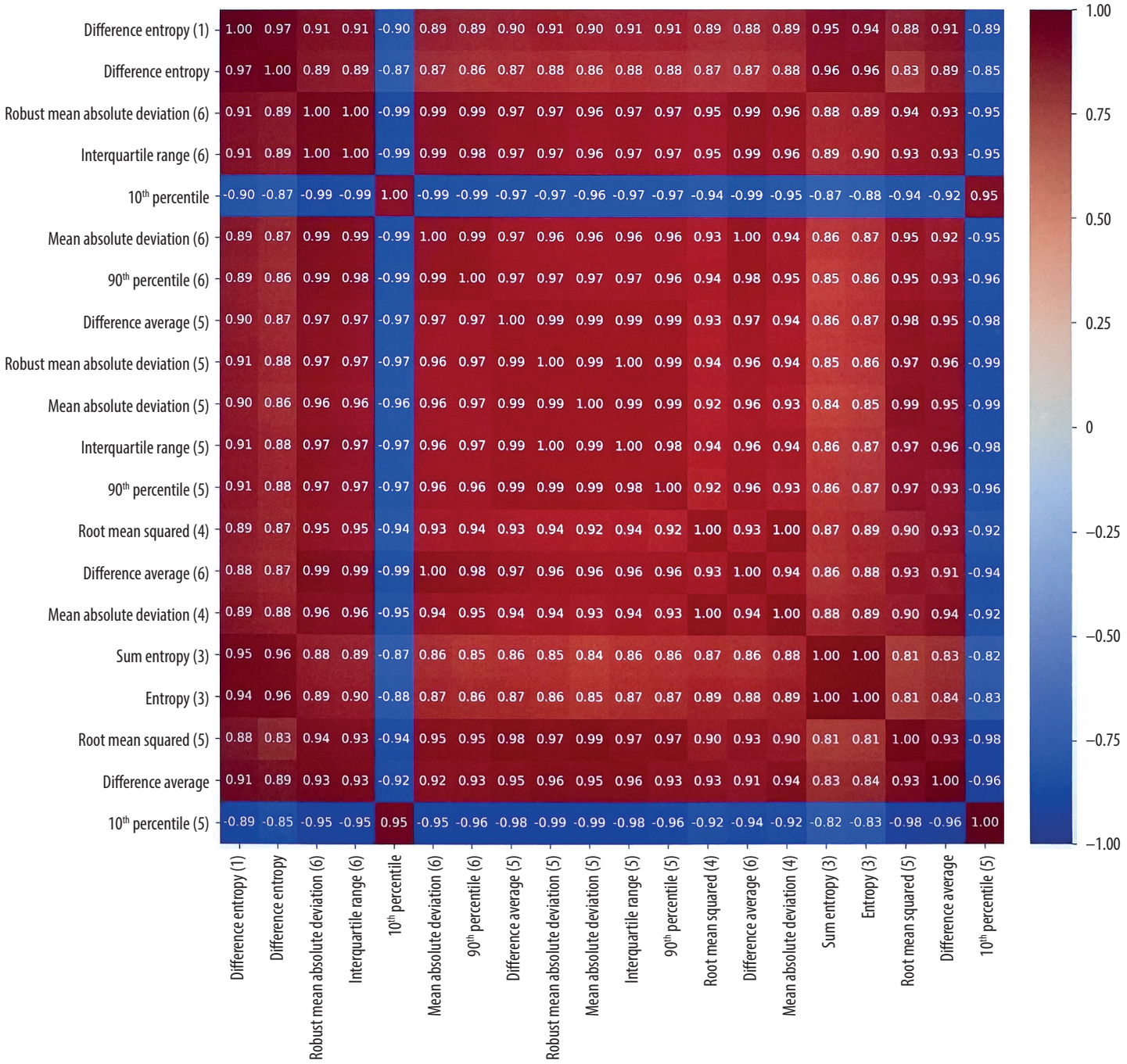

Figure 5. Top 20 Correlated Features

of GLCM-based texture features provided detailed insights into tumor heterogeneity and biologically relevant imaging biomarkers. The use of LASSO reduced feature redundancy and multicollinearity, enhancing model robustness, while the non-invasive approach captures whole-tumor characteristics compared to limited biopsy samples.

Conclusions

Our study demonstrates that multi-sequence MRI-based radiomics, combined with advanced ML classifiers, can effectively differentiate cervical SCC from non-SCC subtypes with unprecedented accuracy. The integration of axial T2WI, sagittal T2WI, and DWI sequences consistently outperformed single-sequence models, with the RF classifier achieving near-perfect ROC-AUC and balanced performance across all evaluation metrics. GLCM-based texture features and other radiomic biomarkers captured subtle yet clinically relevant tumor heterogeneity, highlighting the potential of radiomics to provide biologically meaningful insights beyond conventional imaging. Those underscore the promise of non-invasive, quantitative imaging for precise tumor characterization, potentially guiding personalized management strategies and reducing reliance on invasive biopsies. These results pave the way for future prospective, multi-center studies to validate and expand the clinical applicability of MRI radiomics in cervical cancer.

Disclosures

1. Institutional review board statement: Approval number 2/25/889.
2. Assistance with the article: None.
3. Financial support and sponsorship: None.
4. Conflicts of interest: None.

References

1. Sung H, Ferlay J, Siegel RL, Laversanne M, Soerjomataram I, Jemal A, Bray F. Global cancer statistics 2020: GLOBOCAN estimates of incidence and mortality worldwide for 36 cancers in 185 countries. CA Cancer J Clin 2021; 71: 209-249.
2. Bodurtha Smith AJ, Beavis AL, Rositch AF, Levinson K. Disparities in diagnosis and treatment of cervical adenocarcinoma compared with squamous cell carcinoma: an analysis of the National Cancer Database, 2004-2017. J Low Genit Tract Dis 2023; 27: 29-34.
3. Wu SY, Huang EY, Lin H. Optimal treatments for cervical adenocarcinoma. Am J Cancer Res 2019; 9: 1224-1234.
4. Rajaram S, Gupta B. Screening for cervical cancer: choices & dilemmas. Indian J Med Res 2021; 154: 210-220.
5. Winfield JM, Orton MR, Collins DJ, Ind TEJ, Attygalle A, Hazell S, et al. Separation of type and grade in cervical tumours using non-mono-exponential models of diffusion-weighted MRI. Eur Radiol 2017; 27: 627-636.
6. Haldorsen IS, Lura N, Blaakær J, Fischerova D, Werner HMJ. What is the role of imaging at primary diagnostic work-up in uterine cervical cancer? Curr Oncol Rep 2019; 21: 77. DOI: 10.1007/s11912-019-0824-0.
7. Bhatla N, Berek JS, Cuello Fredes M, Denny LA, Grenman S, Karunaratne K, et al. Revised FIGO staging for carcinoma of the cervix uteri. Int J Gynaecol Obstet 2019; 145: 129-135.
8. McCague C, Ramlee S, Reinius M, Selby I, Hulse D, Piyatissa P, et al. Introduction to radiomics for a clinical audience. Clin Radiol 2023; 78: 83-98.
9. Liu H, Lao M, Zhang Y, Chang C, Yin Y, Wang R. Radiomics-based machine learning models for differentiating pathological subtypes in cervical cancer: a multicenter study. Front Oncol 2024; 14: 1346336. DOI: 10.3389/fonc.2024.1346336.
10. Sun J, Wu G, Shan F, Meng Z. The value of IVIM DWI in combination with conventional MRI in identifying the residual tumor after cone biopsy for early cervical carcinoma. Acad Radiol 2019; 26: 1040-1047.
11. Yoon A, Park JJ, Park BK, Lee YY, Paik ES, Choi CH, et al. Long-term outcomes of MRI stage IIB cervical cancer. Int J Gynecol Cancer 2016; 26: 1252-1257.
12. Tibshirani R. Regression shrinkage and selection via the lasso: a retrospective. J R Stat Soc Ser B Stat Methodol 2011; 73: 273-282.
13. Gökmen Inan N, Kocadağlı O, Yıldırım D, Meşe İ, Kovan Ö. Multi-class classification of thyroid nodules from automatic segmented ultrasound images: Hybrid ResNet based UNet convolutional neural network approach. Comput Methods Programs Biomed 2024; 243: 107921. DOI: 10.1016/j.cmpb.2023.107921.
14. Gala FB, Gala KB, Gala BM. Magnetic resonance imaging of uterine cervix: a pictorial essay. Indian J Radiol Imaging 2021; 31: 454-467.
15. Baliyan V, Das CJ, Sharma R, Gupta AK. Diffusion weighted imaging: technique and applications. World J Radiol 2016; 8: 785-798.
16. Manganaro L, Lakhman Y, Bharwani N, Gui B, Gigli S, Vinci V, et al. Staging, recurrence and follow-up of uterine cervical cancer using MRI: updated guidelines of the European Society of Urogenital Radiology after revised FIGO staging 2018. Eur Radiol 2021; 31: 7802-7816.
17. Davnall F, Yip CSP, Ljungqvist G, Selmi M, Ng F, Sanghera B, et al. Assessment of tumor heterogeneity: an emerging imaging tool for clinical practice? Insights Imaging 2012; 3: 573-589.
18. O'Connor JPB, Rose CJ, Waterton JC, Carano RAD, Parker GJM, Jackson A. Imaging intratumor heterogeneity: role in therapy response, resistance, and clinical outcome. Clin Cancer Res 2015; 21: 249-257.
19. Ryu SY, Kim MH, Nam BH, Lee TS, Song ES, Park CY, et al. Intermediate-risk grouping of cervical cancer patients treated with radical hysterectomy: a Korean Gynecologic Oncology Group study. Br J Cancer 2014; 110: 278-285.
20. Abu-Rustum NR, Yashar CM, Arend R, Barber E, Bradley K, Brooks R, et al. NCCN guidelines® insights: cervical cancer, version 1.2024. J Natl Compr Canc Netw 2023; 21: 1224-1233.
21. Kuang F, Ren J, Zhong Q, Liyuan F, Huan Y, Chen Z. The value of apparent diffusion coefficient in the assessment of cervical cancer. Eur Radiol 2013; 23: 1050-1058.
22. Mabuchi S, Okazawa M, Matsuo K, Kawano M, Suzuki O, Miyatake T, et al. Impact of histological subtype on survival of patients with surgically-treated stage IA2-IIB cervical cancer: adenocarcinoma versus squamous cell carcinoma. Gynecol Oncol 2012; 127: 114-120.
23. Shibata K, Kajiyama H, Yamamoto E, Terauchi M, Ino K, Nomura S, et al. Effectiveness of preoperative concurrent chemoradiation therapy (CCRT) for locally advanced adenocarcinoma of cervix. Eur J Surg Oncol 2009; 35: 768-772.
24. Lin Y, Li H, Chen Z, Ni P, Zhong Q, Huang H, Sandrasegaran K. Correlation of histogram analysis of apparent diffusion coefficient with uterine cervical pathologic finding. AJR Am J Roentgenol 2015; 204: 1125-1131.
25. Chung JJ, Kim MJ, Cho NH, Park S, Lee JT, Yoo HS. T2-weighted fast spin-echo MR findings of adenocarcinoma of the uterine cervix: comparison with squamous cell carcinoma. Yonsei Med J 1999; 40: 226-231.
26. Tsujikawa T, Rahman T, Yamamoto M, Yamada S, Tsuyoshi H, Kiyono Y, et al. ^{18}F-FDG PET radiomics approaches: comparing and clustering features in cervical cancer. Ann Nucl Med 2017; 31: 678-685.
27. Shen WC, Chen SW, Liang JA, Hsieh TC, Yen KY, Kao CH. [18]Fluorodeoxyglucose positron emission tomography for the textural features of cervical cancer associated with lymph node metastasis and histological type. Eur J Nucl Med Mol Imaging 2017; 44: 1721-1731.
28. Downey K, Riches SF, Morgan VA, Giles SL, Attygalle AD, Ind TE, et al. Relationship between imaging biomarkers of stage I cervical cancer and poor-prognosis histologic features: quantitative histogram

analysis of diffusion-weighted MR images. AJR Am J Roentgenol 2013; 200: 314–320.
29. Kido A, Mikami Y, Koyama T, Kataoka M, Shitano F, Konishi I, Togashi K. Magnetic resonance appearance of gastric-type adenocarcinoma of the uterine cervix in comparison with that of usual-type endocervical adenocarcinoma: a pitfall of newly described unusual subtype of endocervical adenocarcinoma. Int J Gynecol Cancer 2014; 24: 1474-1479.
30. Ando H, Miyamoto T, Kashima H, Takatsu A, Ishii K, Fujinaga Y, et al. Usefulness of a management protocol for patients with cervical multicystic lesions: a retrospective analysis of 94 cases and the significance of GNAS mutation. J Obstet Gynaecol Res 2016; 42: 1588-1598.
31. Saida T, Sakata A, Tanaka YO, Ochi H, Ishiguro T, Sakai M, et al. Clinical and MRI characteristics of uterine cervical adenocarcinoma: its variants and mimics. Korean J Radiol 2019; 20: 364-377.
32. Avanzo M, Stancanello J, El Naqa I. Beyond imaging: the promise of radiomics. Phys Med 2017; 38: 122-139.
33. Wang W, Jiao Y, Zhang L. Multiparametric MRI-based radiomics analysis: differentiation of subtypes of cervical cancer in the early stage. Acta Radiol 2022; 63: 847-856.
34. Wang S, Jiang T, Hu X, Hu H, Zhou X, Wei Y, et al. Can the combination of DWI and T2WI radiomics improve the diagnostic efficiency of cervical squamous cell carcinoma? Magn Reson Imaging 2022; 92: 197-202.
35. Feng Q, Chen Y, Liao Z, Jiang H, Mao D, Wang M, et al. Corpus callosum radiomics-based classification model in Alzheimer's disease: a case-control study. Front Neurol 2018; 9: 618. DOI: 10.3389/fneur.2018.00618.